Crashworthiness design for functionally graded foam-filled thin-walled structures

Article *in* Materials Science and Engineering A · March 2010

DOI: 10.1016/j.msea.2009.11.022

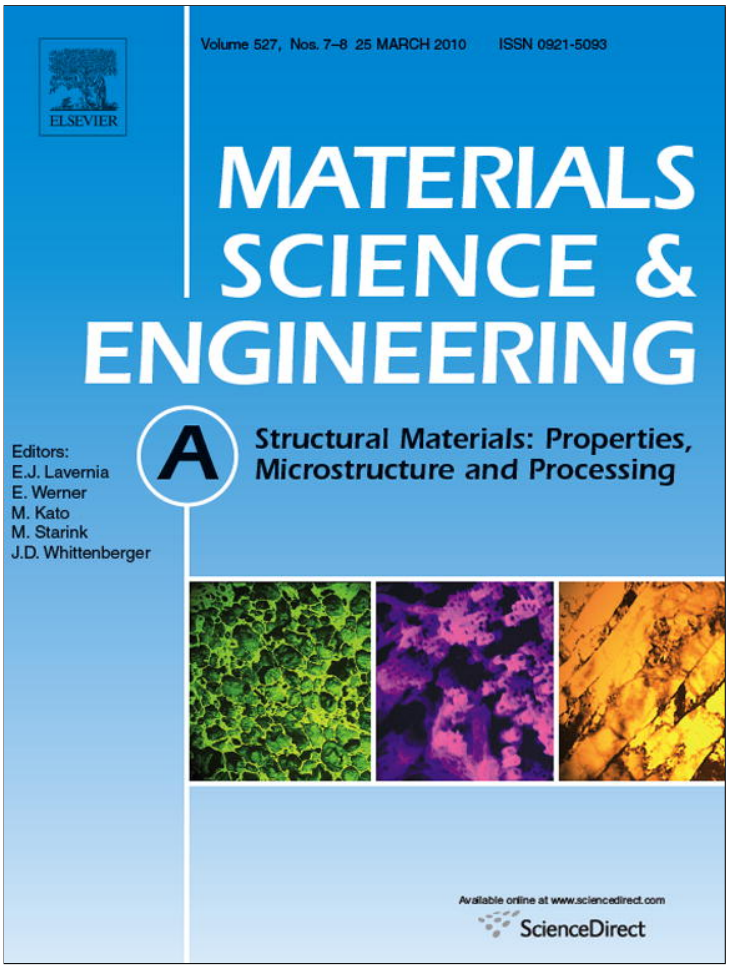

Materials Science and Engineering A 527 (2010) 1911–1919

Contents lists available at ScienceDirect

Materials Science and Engineering A

journal homepage: www.elsevier.com/locate/msea

Crashworthiness design for functionally graded foam-filled thin-walled structures

Guangyong Sun[a,b], Guangyao Li[a], Shujuan Hou[a], Shiwei Zhou[b], Wei Li[b], Qing Li[b,*]

[a] State Key Laboratory of Advanced Design and Manufacture for Vehicle Body, Hunan University, Changsha 410082, China
[b] School of Aerospace, Mechanical and Mechatronic Engineering, Faculty of Engineering, The University of Sydney, Sydney, NSW 2006, Australia

ARTICLE INFO

Article history:
Received 11 August 2009
Received in revised form 6 November 2009
Accepted 9 November 2009

Keywords:
Design optimization
Functionally graded materials (FGM)
Foam-filler
Multiobjective optimization
Crashworthiness
Response surface method
Thin-wall structure

ABSTRACT

Foam-filled thin-wall structures have exhibited significant advantages in light weight and high energy absorption and been widely applied in automotive, aerospace, transportation and defence industries. Unlike existing uniform foam materials, this paper introduces functionally graded foam (FGF) fillers to fill thin-walled structures, aiming to improve crashworthiness. In this novel structure, the foam density varies throughout the depth in a certain gradient. Numerical simulations showed that gradient exponential parameter *m* that controls the variation of foam density has significant effect on system crashworthiness. In this study, the single and multiobjective particle swarm optimization methods are used to seek for optimal gradient, where response surface models are established to formulate specific energy absorption and peak crushing force. The results yielded from the optimizations indicate that the FGF material is superior to its uniform counterparts in overall crashworthiness. The data has considerable implication in design of FGF materials for optimizing structural crashworthiness.

1. Introduction

Thin-walled structures have been widely used as energy absorbers in crashworthiness applications such as automobile and aeronautical industries to protect passenger from severe injury. The early investigation of energy absorbers concentrated on steel columns for their low costs and excellent ductility [1]. As the increasing importance of mass reduction, the use of aluminum columns has become more and more predominant in the recent years [2]. To better understand crashing behaviours of aluminum columns, comprehensive studies have been conducted by using analytical, numerical and experimental methods. For example, Wierzbicki and Abramowicz [3] derived a close-form formula to calculate the axial crush response of aluminum thin-walled columns and this model was validated experimentally by Abramowicz and Jones [4,5] and Langseth and Hopperstad [6].

The impacting structures are expected to absorb maximum energy during crash with minimum mass, in which the specific energy absorption (SEA) is often regarded as an effective measure of such characteristics [7–9]. To achieve light weight design, cellular materials like metal foams have exhibited especially superior capability of absorbing impact energy while they are severely deformed. For this reason, the inclusion of lightweight foam-fillers into thin-walled structures has drawn increasing attention recently. The literature has proven that foam materials are indeed ideal energy absorbers because they can undergo large deformation at nearly constant load. The presence of the foam-filler materials in thin-walled structure helps improve crushing stability and collapse mode of the structure, thereby increasing the overall crashworthiness [10]. In this regard, substantial effort has been devoted on the effect of foam-filler on the energy absorption characteristics of circular and squared thin-walled tubes. For example, Reid et al. [11,12] performed a comprehensive experimental study on the crushing behaviour of squared foam-filled columns under quasi-static and dynamic loadings. Hanssen et al. [13,14] presented the close-form formulas to predict the responses of aluminum columns filled with aluminum foam under both quasi-static and dynamic axial loading conditions. Santosa and Wierzbicki [15] investigated the effect of aluminum honeycomb filler on the axial crushing resistance of a squared box column, which showed that filling the box column with aluminum honeycomb can be more preferable over thickening the column wall.

Although foam-filled thin-walled tubes are able to enhance the energy absorption capacity, the energy absorption was found to be highly dependent on the foam density, where the higher the foam density, the higher the energy absorption. Seitzberger et al. [16] pointed out that filling the thin-walled circular tube with high-density foam could lead to global buckling. In another study, Reyes

* Corresponding author. Tel.: +61 2 9351 8607; fax: +61 2 9351 8607.
E-mail address: Q.Li@usyd.edu.au (Q. Li).

0921-5093/$ – see front matter © 2009 Published by Elsevier B.V.
doi:10.1016/j.msea.2009.11.022

et al. [17] found that high-density aluminum foam could increase the energy absorption of thin-walled square tube considerably, but the specific energy absorption can be lowered compared with the empty tube. It appears common that filling thin-wall circular and square tubes with high-density foam may cause a reduction in SEA [10]. For this reason, the selection of tube geometry and appropriate foam density are critical to optimize the crashworthiness of such structures. In this regard, Hou et al. [18] utilized single and multiple crashworthiness criteria to optimize the square thin-walled column with aluminum foam-filler. Zarei and Kroger [19,20] used multicriteria design optimization (MDO) technique to maximize the energy absorption and minimize the weight of foam-filled aluminum tubes. Nariman-Zadeh et al. [21] adopted multiobjective genetic algorithms to minimize the weight and maximize the energy absorption of square aluminum column with aluminum foam-filler.

These abovementioned foam materials are assumed to contain approximately identical microscopic cells/pores. Their overall characteristics are typically assumed to be isotropic and homogenous, namely uniform foam materials. Alternative materials used as energy absorbing structures are laminated composite materials [22]. However, the inter-laminar stresses within laminated materials are localized at interfaces due to strong mismatching between the material properties. This localization of stress can lead to delamination and crack propagation under certain loading [23]. Recently, Gupta fabricated functionally graded syntactic foam and showed experimentally that it can improve the energy absorption [24,25]. Cui et al. [22] presented a functionally graded foam (FGF) material that contains micro-scale cells varied continuously in a predefined manner and they showed that the FGF materials are suitable candidate for improving energy absorbing behaviours over those conventional uniform foams. Kiernan et al. [26] explored the stress wave propagation through artificial FGF materials with various gradient functions. They showed that the amplification of the stress wave and plastic dissipation energy are determined by the gradient functions. Therefore, it is believed that functionally graded foam materials have significant potential to improve the crashworthiness.

Although fabricating a functionally graded foam material could be inherently more sophisticated than making uniform foam, some advanced technologies have been available to produce such materials for a given gradient under laboratory conditions [27–29]. It has been at a point to make use of graded foam materials for energy absorption under impact scenarios. To do so, firstly, it is essential to understand its energy absorption characteristics in comparison with those generated by well-studied conventional uniform foam material. Secondly, it is of particular significance to seek the best possible foam gradient for optimizing crashworthiness under multiple criteria.

This paper aims at addressing these two critical issues by considering the FGF filled square thin-wall column. A layered finite element model is developed to approximate the graded foam in terms of a power law determined by exponent m. The effect of gradient parameter m on the crashworthiness is explored. The single- and multiobjective optimizations are then carried out by using the particle swarm optimization algorithm to provide a better understanding how different crashworthiness criteria interact each other [18]. The results demonstrated that the columns filled by the graded foam provide a better crashworthiness performance than the uniform counterpart.

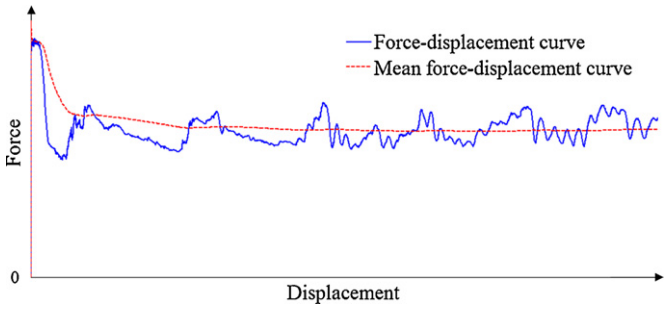

Fig. 1. Axial impact force versus displacement in a typical thin-walled structure.

2. Materials and methods

2.1. Crashworthiness indicators

To systematically study the crashworthiness of graded foam-filled thin-walled structures and optimize the performance, it is essential to define the crashworthiness indicator. The force–displacement curves of typical thin-walled structure, as illustrated in Fig. 1, can to a certain extent measure the impact characteristic. The absorbed energy (E) is calculated as:

$$E(d) = \int_0^d F(x)\ dx \tag{1}$$

where d is crash distance. The average force curve (F_{avg}) for a given deformation can be calculated as:

$$F_{avg} = \frac{E(d)}{d} \tag{2}$$

Following Eq. (1), the specific energy absorbed per unit mass has been a key indicator to distinguish energy absorption capabilities of different materials and weights, defined by

$$\text{SEA} = \frac{E}{M} \tag{3}$$

Obviously, the higher the SEA, the better the capability of energy absorption.

2.2. Functionally graded foam-filler material

It is assumed that the square column is filled with functionally graded foam whose direction of density gradient coincides with that of the axial impact velocity. In this study, the density gradient is defined in a power-law function as [22]:

$$\rho_f(y) = \rho_{f1} + (\rho_{f2} - \rho_{f1})\left[\frac{y}{l}\right]^m \tag{4}$$

where ρ_{f1} and ρ_{f2} are the densities at the incident (impacted) and distal (opposite) surfaces, respectively, l the length of foam-filled column, y the distance from incident surface, and m is the parameter that governs the variation of foam density. For the case that the foam density increases along length, the gradient function changes from convex to concave while the m value varies from less than 1 to greater than 1, as shown in Fig. 2. For the case that the foam density decreases along length, on the other hand, an opposite tendency can be formulated. Since an ideal energy absorption crushing patterns is progressive folding from the impact surface, the present paper considers only the cases with increasing density from the incident surface to the distal surface.

Unfortunately, there is no effective constitutive model available for functionally graded foam materials to date. To deal with the issue, the foam is divided into a number of layers along the axial length, in which each layer consists of a homogeneous and isotropic uniform foam material, as reported by Deshpande and Fleck [30].

The yield criterion of each uniform foam material is defined as follows:

$$\Phi = \hat{\sigma} - \sigma_y \le 0 \tag{5}$$

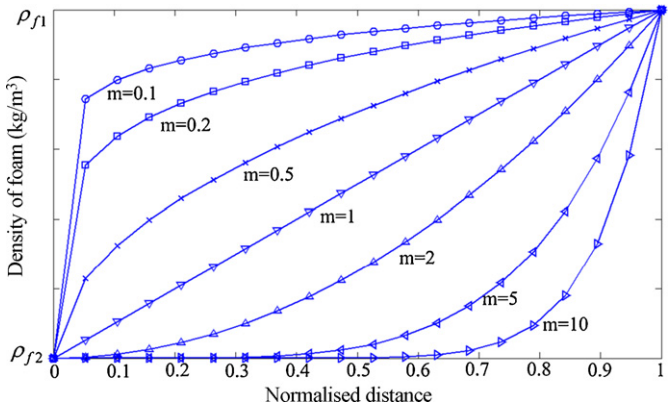

Fig. 2. Variation in density versus normolised distance (0 = incident surface, 1 = distal surface).

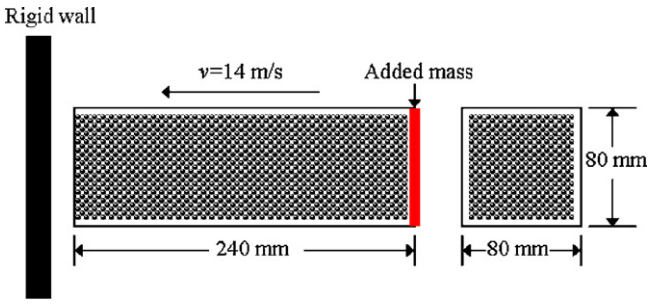

Fig. 3. Geometry dimensions and loading condition.

where σ_y is the yield stress and the equivalent stress $\hat{\sigma}$ is given as:

$$\hat{\sigma}^2 = \frac{1}{[1+(\alpha/3)^2]}[\sigma_e^2 + \alpha^2\sigma_m^2] \tag{6}$$

where σ_e is the von Mises effective stress and σ_m is the mean stress. Parameter α that controls the shape of the yield surface is a function of the plastic Poisson's ratio ν_p given as:

$$\alpha^2 = \frac{9(1-2\nu_p)}{2(1+\nu_p)} \tag{7}$$

It is easily derived from Eq. (7) that $\alpha = 2.12$ when $\nu_p = 0$.

The strain hardening rule is implemented in this material model as:

$$\sigma_y = \sigma_p + \gamma\frac{\hat{\varepsilon}}{\varepsilon_D} + \alpha_2 \ln\left[\frac{1}{1-(\hat{\varepsilon}/\varepsilon_D)^\beta}\right] \tag{8}$$

where $\hat{\varepsilon}$ is equivalent strain, $\sigma_p, \alpha_2, \gamma, \beta$ and ε_D are material parameters and can be related to the foam density as

$$\begin{cases} \left(\sigma_p, \alpha_2, \gamma, \dfrac{1}{\beta}, E_p\right) = C_0 + C_1\left(\dfrac{\rho_f}{\rho_{f0}}\right)^\kappa \\ \varepsilon_D = -\ln\left(\dfrac{\rho_f}{\rho_{f0}}\right) \end{cases} \tag{9}$$

where ρ_f is the foam density and ρ_{f0} is the density of the base material. C_0, C_1 and κ are the constants, listed in Table 1. It is noted that the Young's modulus of foam material E_p is also a function of ρ_f as in Eq. (9) [31].

2.3. Finite element modeling

The structure considered in this paper is a thin-walled square column filled with functionally graded aluminum foam, where the sectional dimension is 80 mm × 80 mm × 1.0 mm, and the length is 240 mm. The geometry is determined from typical dimensions of the front side rail of a passenger car [33]. The column impacts onto the rigid wall at an initial velocity of 14 m/s. To generate enough kinetic energy, an additional mass of 460 kg is attached to the right end of the column as in Fig. 3.

The material of the wall column used here is aluminum alloy AA6061-T4 with mechanical properties of density $\rho = 2.7 \times 10^3$ kg/m^3, Young's modulus $E = 68.2$ GPa, Poisson's ratio $\nu = 0.30$, initial yielding stress $\sigma_{y0} = 80$ MPa, ultimate strength $\sigma_u = 173$ MPa, and the exponent $n = 0.23$ [34]. The constitutive relation is based on an elastic–plastic material model with von Mises's isotropic plasticity algorithm and plastic hardening.

The finite element model for the thin-wall square column filled with functionally graded aluminum foam was developed in LS-DYNA 970 that is considered appropriate to model both material and geometric non-linearities, and is particularly suitable for simulating impact problems. In this study, Belytschko–Lin–Tsay reduced integration shell elements were used to model the column wall. Three integration points were used through the thickness and one integration point in the plane of the elements. To model the foam material, the eight-node brick elements with one-point reduced integration were used. The foam core is divided into 20 layers along the axial length. Each layer assigned a unique value of ρ_f as defined in the gradient functions as dotted in Fig. 2. Based on the density value ρ_f, the other material properties can be calculated from Eq. (9). After undertaking a convergence study, an element size of 3 mm was found to produce suitable results. The same conclusion had been drawn by Aktay et al. [35] in a similar structure. Therefore, the side lengths of square and cube elements in the tube wall and foam were both 3 mm. As with all reduced integration elements, the hourglass control was employed to eliminate spurious zero-energy modes commonly arising when reduced integration elements are used.

Since the foam-filled tube consists of two different materials, different contact algorithms in LS-DYNA have to be used. The interface between the foam and column wall was modeled with an automatic surface to surface contact. Automatic single surface contact was also applied to the column walls to avoid interpenetration of folding generated during axial collapse [36]. Finally, node to surface contact was used between the impact surface of the column and the rigid wall. Contact stiffness for each contact pair was selected such that neither interpenetration, resulting from low stiffness values, nor instability, commonly occurring in excessively high stiffness values, is encountered.

According to the above description, the 3D finite element model is shown in Fig. 4.

Table 1
Material constants for aluminum foam [31,32].

	σ_p (MPa)	α_2 (MPa)	$1/\beta$	γ (MPa)	E_p (MPa)
C_0 (MPa)	0	0	0.22	0	0
C_1 (MPa)	720	140	320	42	0.33E6
κ	2.33	0.45	4.66	1.42	2.45

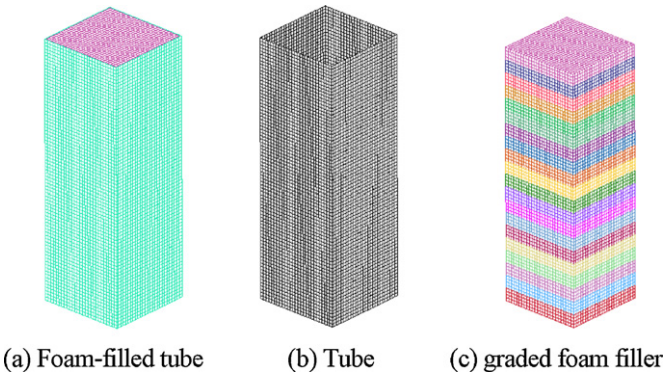

Fig. 4. 3D finite element modeling of graded foam-filled column. (a) Foam-filled tube, (b) tube, and (c) graded foam-filler.

2.4. Design optimization model

To optimize the crashworthiness of the FGF filled thin-walled structure, design optimization will be applied. In automotive scenarios, the impact force peak, F_{max}, is critical to the occupant survival rate when impact occurs. An overly high F_{max} often leads to severe injury or even death of occupant. In this study, F_{max} is chosen as either a constraint or an objective in a single objective optimization framework, while $F_{\max}$ is taken as one objective function in the multiobjective optimization framework.

To account for these different design schemes mentioned above, the optimization problem can be formulated in the following two different ways:

- **Case 1**: Single objective optimization

The maximization of SEA is selected as the objective while $F_{\max}$ is taken as the constraint:

$$\begin{cases} \text{Maximize} & \text{SEA}(m) \\ \text{s.t.} & F_{\max}(m) \le F_{\text{const}} \\ & m^L \le m \le m^U \end{cases} \tag{10}$$

or $F_{\max}$ is taken as the objective while SEA as the constrain, given by:

$$\begin{cases} \text{Minimize} & F_{\max}(m) \\ \text{s.t.} & \text{SEA}(m) \ge \text{SEA}_{\text{const}} \\ & m^L \le m \le m^U \end{cases} \tag{11}$$

where F_{const} is the upper limit of crash force, $\text{SEA}_{\text{const}}$ the lower limit of SEA, m^L and m^U are the lower limit and upper limit of gradient parameter m, respectively.

- **Case 2**: Multiobjective optimization

The maximizations of SEA and reverse force peak are presented in a multiobjective framework:

$$\begin{cases} \text{Maxmize} & [\text{SEA}(m), -F_{\max}(m)] \\ \text{s.t.} & m^L \le m \le m^U \end{cases} \tag{12}$$

It should be pointed out that, however, it is by no means easy to mathematically define SEA and $F_{\max}$ in Eqs. (10)–(12). As an effective alternative, the surrogate or metamodel techniques have been widely adopted in crashworthiness design. In the study, the response surface method is exploited to approximate the objective and constraint functions [37].

The general form of response surface model can be expressed as:

$$y = \tilde{y} + \varepsilon = \sum_{l=1}^{L} a_l \varphi_l(\mathbf{x}) + \varepsilon \tag{13}$$

where y denotes the FEA result, $\tilde{y}$ the response surface model, ε comprises bias and random errors, $\mathbf{x}$ denotes design variables,

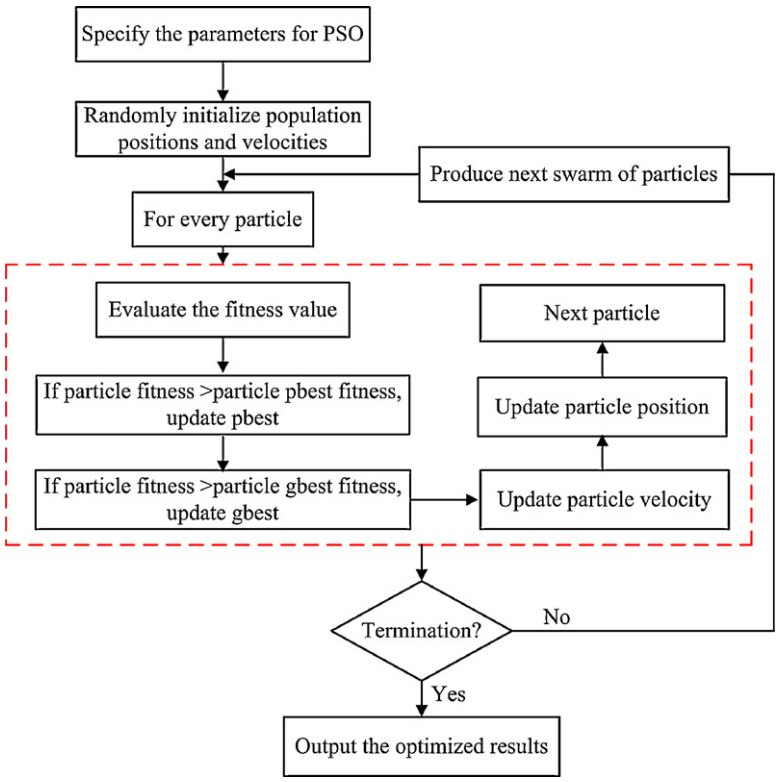

Fig. 5. The flowchart of PSO algorithm.

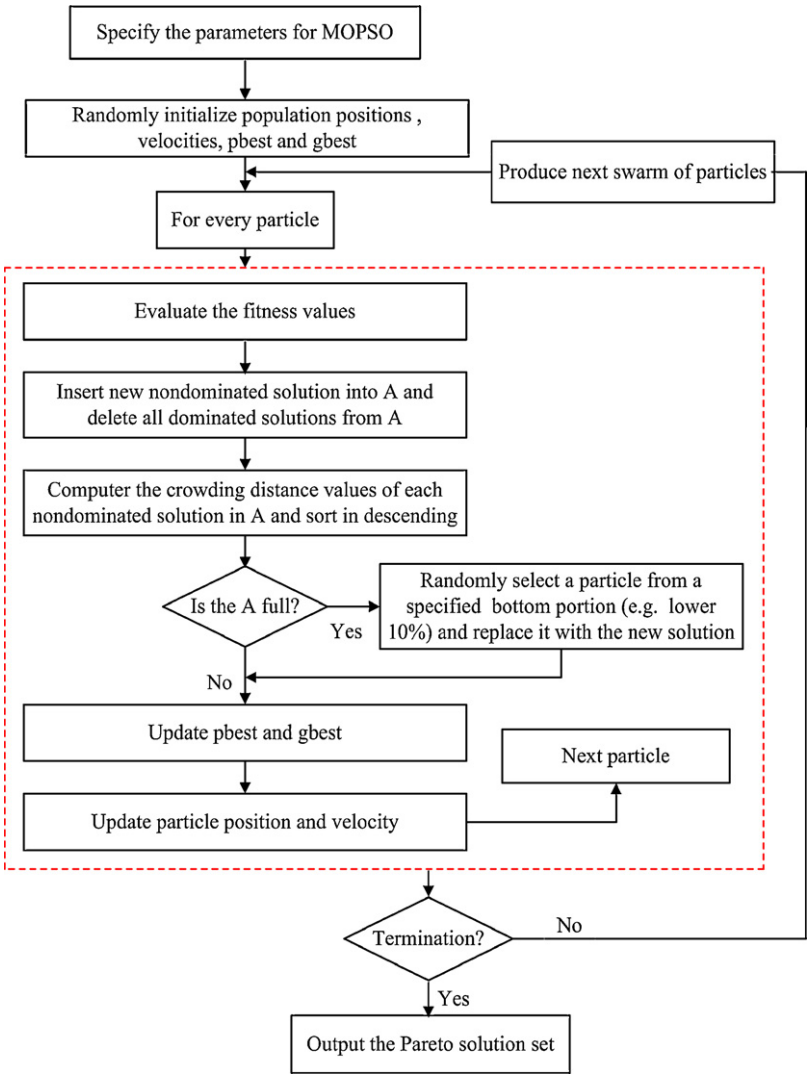

Fig. 6. The flowchart of MOPSO algorithm.

and a_l ($l = 1, \ldots, L$) stands for the lth unknown coefficient corresponding to the lth basis function $\varphi_l(\mathbf{x})$. In theory, the basis function can be any form of function, while in most cases, polynomial functions have proven effective.

If the analysis results $\boldsymbol{y} = [y^{(1)}, y^{(2)}, \ldots, y^{(P)}]^T$ at selected P sample design points ($P \geq L$) are obtained, the unknown parameters $\boldsymbol{a} = [a_1, a_2, \ldots, a_L]^T$ can be determined by means of the least squares method [38]. At the ith design point $\mathbf{x}_i$, the error between the analysis and approximation is expressed as

$$\varepsilon_i = y^{(i)} - \tilde{y}^{(i)} = y^{(i)} - \sum_{i=1}^{L} a_l \varphi_l(\mathbf{x}_i) \tag{14}$$

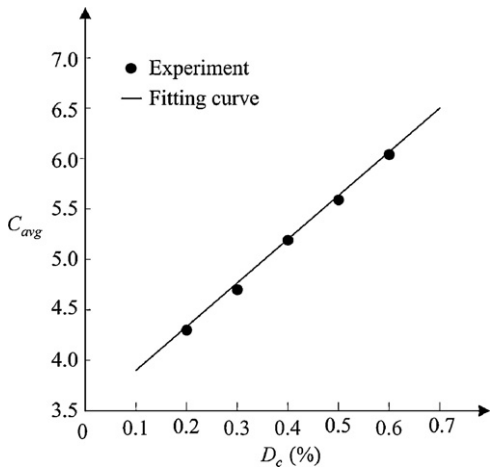

Fig. 7. Interaction as a function of deformation [49].

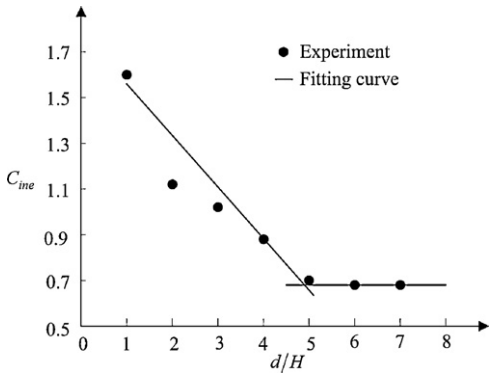

Fig. 8. Dynamic amplification as a function of relative lobe deformation [49].

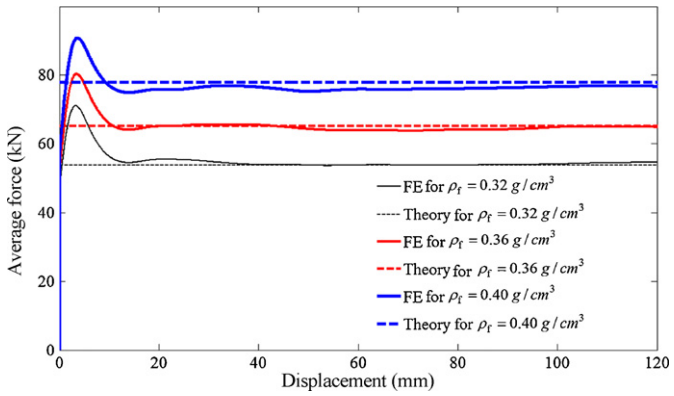

Fig. 9. Average load versus deflection curves for the foam-filled tubes.

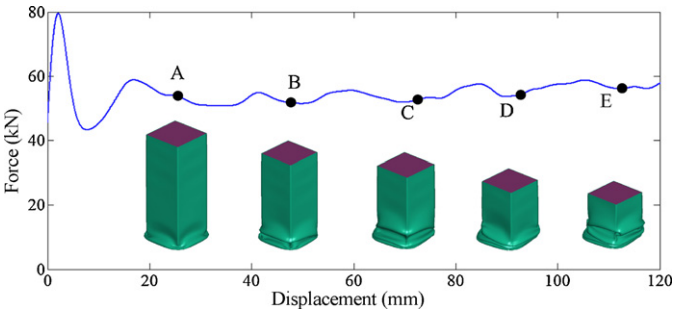

Fig. 10. Axial crushing behaviour of foam-filled tube (rigid wall on the bottom of the columns).

and the sum of the squared errors $E(\boldsymbol{a})$ at these P selected design points is given as:

$$E(\boldsymbol{a}) = \sum_{i=1}^{P} \varepsilon_i^2 = \sum_{i=1}^{P} \left[y^{(i)} - \sum_{i=1}^{L} a_l \varphi_l(\mathbf{x}_i) \right]^2 \tag{15}$$

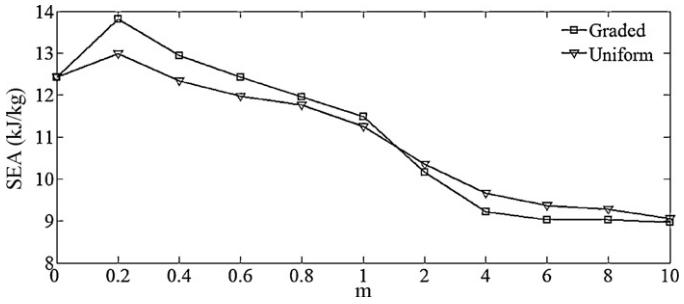

Fig. 11. Relationships between SEA and m.

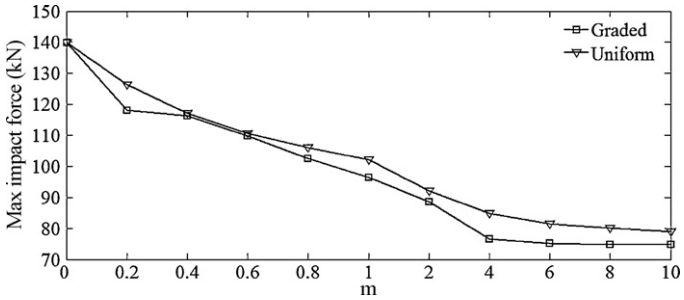

Fig. 12. Relationships between impact force peak and m.

Table 2
Optimization results of maximizing SEA with F_{max} constraint.

	Optimal m	Max. SEA (kJ/kg)	F_{max} (kN)
Graded foam-filled column	0.1389	13.8527	121.0664
Uniform foam-filled column	0.1826	12.8578	127.1247

Table 3
Optimization results of minimizing F_{max} with SEA constraint.

	Optimal m	Min. F_{max} (kN)	SEA (kJ/kg)
Graded foam-filled column	0.7829	101.9462	12
Uniform foam-filled column	0.5685	111.3486	12

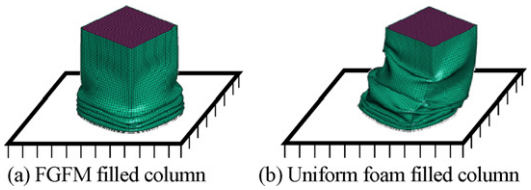

Fig. 13. Deformation mode of foam-filled column with $m = 0.1389$. (a) FGFM filled column and (b) uniform foam-filled column.

Eq. (15) can also be expressed equivalently in a matrix form as:

$$E(\boldsymbol{a}) = \varepsilon^T \varepsilon = (\boldsymbol{y} - \boldsymbol{\varphi a})^T (\boldsymbol{y} - \boldsymbol{\varphi a}) \tag{16}$$

By minimizing $E(\boldsymbol{a})$, the following expressions are obtained:

$$\frac{\partial E(\boldsymbol{a})}{\partial \boldsymbol{a}} = -2\boldsymbol{\varphi}^T \boldsymbol{y} + 2\boldsymbol{\varphi}^T \boldsymbol{a} = 0, \quad \boldsymbol{a} = (\boldsymbol{\varphi}^T \boldsymbol{\varphi})^{-1} \boldsymbol{\varphi}^T \boldsymbol{y} \tag{17}$$

where $\boldsymbol{\varphi}$ is the matrix consisting of basis functions evaluated at all these design points as:

$$\boldsymbol{\varphi} = \begin{bmatrix} \varphi_1(\boldsymbol{x}_1) & \cdots & \varphi_L(\boldsymbol{x}_1) \\ \vdots & \ddots & \vdots \\ \varphi_1(\boldsymbol{x}_P) & \cdots & \varphi_L(\boldsymbol{x}_P) \end{bmatrix} \tag{18}$$

2.5. Particle swarm optimization

The single objective particle swarm optimization or multiobjective particle swarm optimization can be applied to search for an optimum for the problems defined as Eqs. (10)–(12). Inspired by the emergent motion of a flock of birds and fish searching for food, the particle swarm optimization (PSO) method was introduced by

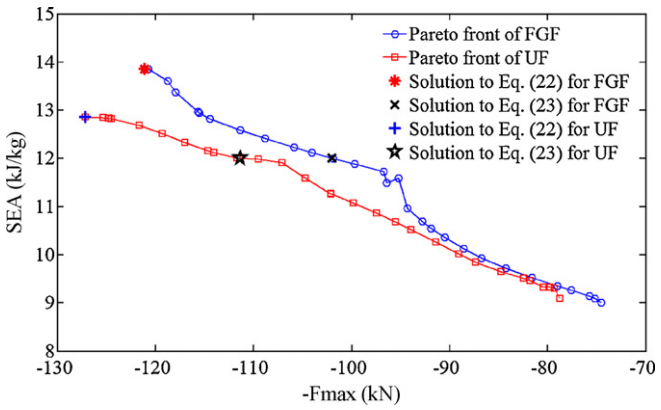

Fig. 14. Pareto fronts of foam-filled columns.

Eberhart and Kennedy [39]. Due to its simplicity in implementation and high computational efficiency, it has been used in a range of applications, e.g. neutral network, pattern recognition, fuzzy system control and other fields [40–45]. The PSO method has been shown in certain instances to outperform other stochastic optimization methods [46].

In PSO, each particle represents a candidate solution associated with two vectors, namely position ($\mathbf{X}_i$) and velocity ($\mathbf{V}_i$). In the b-dimensional search space, the position of particle i at iteration t can be represented in $\boldsymbol{X}_i^t = (x_{i1}^t, x_{i2}^t, \ldots, x_{ib}^t)$, the velocity of particle i at iteration t can be described as $\boldsymbol{V}_i^t = (v_{i1}^t, v_{i2}^t, \ldots, v_{ib}^t)$. Let $\boldsymbol{P}_i^t = (p_{i1}^t, p_{i2}^t, \ldots, p_{ib}^t)$ denote personal best (pbest) which is the best solution that particle i has obtained until iteration t, and $\boldsymbol{P}_g^t = (p_{g1}^t, p_{g2}^t, \ldots, p_{gb}^t)$ represents the global best (gbest) which is the best solution obtained from $\boldsymbol{P}_i^t$ in the population until iteration t. To search for the optimal solution, each particle updates its velocity and position according to following equation:

$$\begin{cases} \boldsymbol{V}_i^{t+1} = w\boldsymbol{V}_i^t + c_1\chi_1(\boldsymbol{P}_i^t - \boldsymbol{X}_i^t) + c_2\chi_2(\boldsymbol{P}_g^t - \boldsymbol{X}_i^t) \\ \boldsymbol{X}_i^{t+1} = \boldsymbol{X}_i^t + \boldsymbol{V}_i^{t+1} \end{cases} \tag{19}$$

where c_1 and c_2 are the acceleration factors, χ_1 and χ_2 are the uniform random numbers in range (0, 1), w is the inertia weight that controls the influence of previous velocity in the new velocity. Fig. 5 gives a flowchart for summarizing the PSO algorithm.

As an extension to PSO, the multiobjective particle swarm optimization (MOPSO) has drawn considerable attention recently because of its relatively fast convergence and well-distributed Pareto front compared with other multiobjective optimization algorithms, such as NSGA, PEAS, etc. [47,48]. A flowchart showing the procedure of MOPSO is provided in Fig. 6. The more details of MOPSO can be also consulted from literature [48].

3. Results and discussion

3.1. Validation of the FE model

The finite element model of the FGF filled tube cannot be directly validated as the experimental data have yet to be reported adequately. Nevertheless, it is possible to validate the numerical modeling results of uniform foam-filler in a special case of FGF with $m = 0$, against those reported in literature. For the uniform foam-filler, Hanssen et al. [49] conducted substantial experimental studies to understand the crash behaviours of uniform density foam-filled column subjected to axial impact and developed a close-form formula for the average impact force, as

$$F_{avg} = 13.06\sigma_0 b_m^{1/3} t^{5/3} \left\{ 1 + C_{ine} \left[\frac{b_m}{t} \frac{\rho}{\sigma_0} v_0^2 \right]^{1/2} \right\} + \sigma_p b_i^2 + C_{avg} \sqrt{\sigma_p \sigma_0} b_m t \tag{20}$$

where σ_0 is characteristic stress of tube material, b_m the inner sectional width, t the thickness of the column wall, b_i the width of the foam core, σ_p the foam plateau stress, and v_0 is the initial velocity. The interaction constant C_{avg} is given in Fig. 7 as a function of deformation, where the relative deformation D_c is given as deformed distance d divided by original component length l. Dynamic amplification C_{ine} is a function of relative lobe length d/H as given in Fig. 8 for the non-filled column. Abramowicz and Jones [5] formulated the half lobe length H as

$$H = 0.99 b_m^{2/3} t^{1/3} \tag{21}$$

It can be seen from Eq. (20) that F_{avg} consists of three parts. The first part is the average crushing force of non-filled column under dynamic loading condition. The second part is the uniaxial resistance of the foam core which neglects the loading rate. The third part indicates the interaction between the foam-filler and the column wall, increasing the crush force.

The finite element models of the FGF filled tube ($m = 0$) can be verified against the results in Eq. (20). Fig. 9 shows the average load versus deflection curves of the foam-filled square tubes obtained from the present FE analysis and empirical models at $\rho_f = 0.32, 0.36, 0.4\ \mathrm{g/cm^3}$, which showed a pretty good agreement. This satisfactory correlation provides adequate confidence in extending the uniform foam-filler model to the FGF filler models, which enable us to conduct design optimization. Fig. 10 shows the force versus crushing displacement of a foam-filled tube ($\rho_f = 0.32\ \mathrm{g/cm^3}$). As expected, the force–displacement curve has a peak value at the beginning of crush and then some oscillations due to the creation of new folds.

3.2. Crashworthiness comparison of uniform and graded foam-filled column

In the present work, a group of graded and uniform foam-filled columns with the same weight were compared for energy absorption characteristics. In each case, the wall thickness is 1.0 mm and the impact duration is 10 ms. The functionally graded foam-filled tubes with different parameters of $m = 0$, 0.2, 0.4, 0.6, 0.8, 1, 2, 4, 6, 8 and 10 were adopted to explore the crashworthiness. To be consistent, the densities of all graded foam-filled tubes at the incident and distal surface are $0.3\ \mathrm{g/cm^3}$ and $0.5\ \mathrm{g/cm^3}$, respectively. Corresponding foam density was selected for uniform foam-filled tubes to keep the same weight as the FGF tubes in different parameters m. In other words, the foam density of uniform foam-filled tubes can be expressed in term of m hereafter. Obviously, the foam densities of uniform foam-filled tubes monotonously increase with decreasing m, reaching the highest density $0.5\ \mathrm{g/cm^3}$ when $m = 0$.

Fig. 11 plots the relationship between SEA and m, from which it can be seen that SEA of the FGF filled column is greater than that of the corresponding uniform foam-filled column when m is less than 1. However, an opposite result is observed when m is greater than 1. For the FGF filled columns, obviously, parameter m that controls the variation of foam density has significant influence on SEA. SEA monotonously increases in the region of m less than 0.2, while in the region of m greater than 0.2, SEA monotonously decreases. The similar trend can be observed for the uniform foam-filled column.

Fig. 12 shows the relationship between the force peak and gradient parameter m. The maximum forces of uniform foam-filled column and graded foam-filled column both decrease with the increase in m. However, the maximum impact force of the graded foam-filled column is relatively lower than that of the uniform counterpart.

Overall, the graded foam-filled columns have a better crashworthiness than the uniform foam-filled column in terms of SEA and peak impact force. Especially, these crashworthiness indicators of the graded foam-filled column are superior when m is less than 1. Therefore, the graded foam-filled column is a potential component in the crashworthiness design. Nevertheless, the variation in foam gradient function has a significant effect on crashworthiness of FGF filled column. Therefore, it would be of great interest to seek best possible m to optimize the crash characteristics of FGF column.

3.3. Single objective optimization

The optimization aims to determine the optimal gradient parameter m to either maximize SEA of the FGF filled column under the constraint of $F_{\max}$ in the single objective optimization, or minimize the peak crash force within the constraints of SEA, specifically as

$$\begin{cases} \text{Maximize} & \text{SEA}(m) \\ \text{s.t.} & F_{\max}(m) \le 130\ \text{kN} \\ & 0 \le m \le 10 \end{cases} \tag{22}$$

or

$$\begin{cases} \text{Minimize} & F_{\max}(m) \\ \text{s.t.} & \text{SEA}(m) \geq 12\,\text{kJ} \\ & 0 \leq m \leq 10 \end{cases} \quad (23)$$

These above two single objective optimization problems are used for the FGF filled and uniform foam-filled thin-walled columns, respectively, to compare their performances. These optimization problems are performed using the PSO algorithm. During the optimization process, the surrogate models of the objective and constraint functions were obtained as in Appendix A. The swarm size chosen was 40, and the PSO was run 100 generations.

Table 2 summarizes the optimal results of m for maximizing SEA with the constraint of $F_{\max}$, from which it can be seen that the optimal SEA of the FGF filled column is higher than that of the uniform counterpart under the same $F_{\max}$ constraint of 130 kN. Table 3 lists the optimal results of minimizing $F_{\max}$ under the SEA constraint, from which it can be found that the minimum $F_{\max}$ of FGF filled column is lower than that of uniform foam-filled column under the same SEA constraint of 12 kJ/kg.

Fig. 13 compares the deformation modes of the optimal graded foam-filled column with $m = 0.1389$ and the corresponding uniform foam-filled column that keeps the same weight as the graded foam-filled column, from which it can be seen that the deformation of graded foam-filled column is more stable than its uniform counterpart.

3.4. Multiobjective optimization

Although the constrained single objective optimization can generate some meaningful results, it lacks an important feature of exploring the interaction of these criteria. From a practical point of view, multiobjective design sometimes appears more sensible. Here, the formulation of multiobjective optimization is given as:

$$\begin{cases} \text{Maxmize} & [\text{SEA}(m), -F_{\max}(m)] \\ \text{s.t.} & 0 \leq m \leq 10 \end{cases} \quad (24)$$

The multiobjective optimization problem is solved using MOPSO. The optimal Pareto fronts of the FGF filled column and uniform foam-filled column are plotted in Fig. 14. It can be clearly seen that the Pareto front of the functionally graded foam-filled column (FGF) is more predominant than that of the uniform foam-filled column (UF). Those optimal single objective results are also depicted in Fig. 14, which can be seen that they only signify some special points in the Pareto front. In other words, the constrained single objective optimization generates only a special solution, while MOPSO obtain a set of solutions.

From Fig. 14, it can be seen the Pareto fronts are not convex, which simply indicate that the use of typical linear weighted method may not be appropriate [18,37]. Here, the MOPSO method proves fairly effective to search for a more sophisticated Pareto front curve.

4. Conclusion

In this paper, a functionally graded foam-filled thin-wall structure is proposed, aiming to improve the energy absorption characteristics offered by uniform foam-filled wall structure. The responses of FGF filled thin-wall column were investigated by using the validated finite element model. A group of graded and uniform foam-filled columns with the same foam weight were compared for energy absorption characteristics. The results showed that SEA of FGF column is greater than that of uniform foam-filled column when $m < 1$, and an opposite result is observed when $m > 1$. The peak impact force of the FGF column is always lower than that of the uniform foam column. The gradient parameter m has a significant effect on the crash characteristics.

To optimize the FGF columns, the constrained single objective and multiobjective optimizations were presented. The particle swarm optimization (PSO) and its multiobjective version (MPSO) were adopted to seek optimal designs for the FGF structures. In the optimization procedure, the response surface method was used to formulate SEA and peak impact force. Optimal results indicated that the FGF filled structure is generally superior to the uniform foam-filled structure. The difference between the single objective and multiobjective optimizations was discussed through observing the Pareto fronts.

It is noted that many natural biological materials, e.g. femur, seashells, cuttlefish bone and bamboos [50] provide extraordinary mechanical properties due to their graded microstructures and compositions. This study is of considerable implications in promoting functionally graded foam materials for applications in crashworthiness and other energy absorption structures.

Acknowledgments

The support from National 973 Project of China (2010CB328005), The Key Project of NSFC (60635020) and The Program for Changjiang Scholar and Innovative Research Team in Chinese Universities are acknowledged. The first author is also grateful the supports from China Scholarship Council (CSC) and School of Aerospace, Mechanical and Mechatronic Engineering, The University of Sydney.

Appendix A. Response surface models

For the design variable m, 11 experimental design points were obtained by continuously increasing from 0 to 1 with an even increment of 0.1, and 10 experimental points by continuously increasing from 2 to 10. Based on these experiment results, functionally graded foam-filled column RSM models of SEA and $F_{\max}$ were established as follows:

$$\text{SEA}^g(m) = \begin{cases} 12.4288 + 25.947317m - 160.85708m^2 + 412.86129m^3 - 538.81804m^4 + 349.35502m^5 - 89.431373m^6 & 0 \leq m \leq 1 \\ 14.2965 - 3.9508999m + 1.3933116m^2 - 0.2866923m^3 + 0.0345840m^4 - 0.0022337m^5 + 5.91 \times 10^{-5} m^6 & 1 < m \leq 10 \end{cases} \quad (A.1)$$

$$F^g_{\max}(m) = \begin{cases} 140.059 - 292.11478m + 1689.4533m^2 - 5104.8986m^3 + 8012.6183m^4 - 6328.5493m^5 + 1979.7574m^6 & 0 \leq m \leq 1 \\ 99.567 + 1.5996698m - 6.4113037m^2 + 1.8843009m^3 - 0.2278144m^4 + 0.0123107m^5 - 2.37 \times 10^{-4} m^6 & 1 < m \leq 10 \end{cases} \quad (A.2)$$

Corresponding uniform foam-filled column RSM models of SEA and $F_{\max}$ were established as follows:

$$\text{SEA}^u(m) = \begin{cases} 12.4232 + 2.2701463m + 25.524476m^2 - 212.25430m^3 + 497.02415m^4 - 479.60436m^5 + 165.87827m^6 & 0 \leq m \leq 1 \\ 12.6969 - 1.6610164m + 0.1736095m^2 + 0.0666918m^3 - 0.0207811m^4 + 0.0021246m^5 - 7.57 \times 10^{-5} m^6 & 1 < m \leq 10 \end{cases} \quad (A.3)$$

$$F^u_{\max}(m) = \begin{cases} 139.903 - 89.296937m + 146.42712m^2 - 288.41745m^3 + 414.87965m^4 - 311.52903m^5 + 90.114379m^6 & 0 \leq m \leq 1 \\ 125.044 - 33.565539m + 13.298855m^2 - 3.0694353m^3 + 0.3999361m^4 - 0.0270845m^5 + 7.38 \times 10^{-4} m^6 & 1 < m \leq 10 \end{cases} \quad (A.4)$$

Table A1
Verification model adequacy.

Fitting indicators	SEA^g		F^g_{max}		SEA^u		F^u_{max}	
	$m \in [0,1]$	$m \in (1,10]$	$m \in [0,1]$	$m \in (1,10]$	$m \in [0,1]$	$m \in (1,10]$	$m \in [0,1]$	$m \in (1,10]$
$R^2 = 1 - \frac{\sum_{i=1}^{P}(y_i - \bar{y}_i)^2}{\sum_{i=1}^{P}(y_i - \bar{y})^2}$	99.67%	99.95%	99.43%	99.77%	98.53%	99.64%	99.99%	99.99%
$R^2_{adj} = 1 - \frac{(1-R^2)(P-1)}{P-p-1}$	99.17%	99.85%	98.58%	99.31%	96.32%	98.91%	99.98	99.99%
$R^2_{pred} = 1 - \frac{\sum_{i=1}^{P}[y_i - \bar{y}_{(i)}]^2}{\sum_{i=1}^{P}(y_i - \bar{y})^2}$	99.02%	99.15%	98.03%	99.21%	96.09%	98.24%	99.71%	99.82%

The verification model adequacy results are summarized in Table A1, from which we found that R^2 and R^2_{adj} of SEA and F_{max} are closed to 1 and these differences between R^2 and R^2_{adj} of SEA and F_{max} are very small, which showed that these response surface models fit experimental design points very well. Therefore, the accuracies of response surface models are adequate to carry on the design optimization.

References

[1] C.P. Gameiro, J. Cirne, International Journal of Mechanical Sciences 49 (9) (2007) 1029–1037.
[2] A. Reyes, O.S. Hopperstad, M. Langseth, International Journal of Solids and Structures 41 (5–6) (2004) 1645–1675.
[3] T. Wierzbicki, W. Abramowicz, Journal of Applied Mechanics-Transactions of the ASME 50 (4A) (1983) 727–734.
[4] W. Abramowicz, N. Jones, International Journal of Impact Engineering 2 (2) (1984) 179–208.
[5] W. Abramowicz, N. Jones, International Journal of Impact Engineering 4 (4) (1986) 243–270.
[6] M. Langseth, O.S. Hopperstad, International Journal of Impact Engineering 18 (7–8) (1996) 949–968.
[7] X. Zhang, G.D. Cheng, Z. You, H. Zhang, Thin-Walled Structures 45 (9) (2007) 737–746.
[8] Y.C. Liu, International Journal of Crashworthiness 13 (5) (2008) 543–550.
[9] Y.C. Liu, Finite Elements in Analysis and Design 44 (3) (2008) 139–147.
[10] Z. Ahmad, D.P. Thambiratnam, Computers & Structures 87 (3–4) (2009) 186–197.
[11] S.R. Reid, T.Y. Reddy, International Journal of Mechanical Sciences 28 (10) (1986) 643–656.
[12] S.R. Reid, T.Y. Reddy, M.D. Gray, International Journal of Mechanical Sciences 28 (5) (1986) 295.
[13] S.P. Santosa, T. Wierzbicki, A.G. Hanssen, M. Langseth, International Journal of Impact Engineering 24 (5) (2000) 509–534.
[14] A.G. Hanssen, M. Langseth, O.S. Hopperstad, International Journal of Impact Engineering 24 (4) (2000) 347–383.
[15] S. Santosa, T. Wierzbicki, Computers & Structures 68 (4) (1998) 343–367.
[16] M. Seitzberger, F.G. Rammerstorfer, H.P. Degischer, R. Gradinger, Acta Mechanica 125 (1–4) (1997) 93–105.
[17] A. Reyes, O.S. Hopperstad, A.G. Hanssen, M. Langseth, International Journal of Impact Engineering 30 (7) (2004) 805–834.
[18] S.J. Hou, Q. Li, S.Y. Long, X.J. Yang, W. Li, Materials & Design 30 (6) (2009) 2024–2032.
[19] H.R. Zarei, M. Kroger, Thin-Walled Structures 46 (2) (2008) 214–221.
[20] H.R. Zarei, M. Kroger, International Journal of Crashworthiness 12 (3) (2007) 255–264.
[21] N. Nariman-Zadeh, A. Darvizeh, A. Jamali, Proceedings of the Institution of Mechanical Engineers Part B-Journal of Engineering Manufacture 220 (2) (2006) 213–224.
[22] L. Cui, S. Kiernan, M.D. Gilchrist, Materials Science and Engineering A-Structural Materials Properties Microstructure and Processing 507 (1–2) (2009) 215–225.
[23] N. Svensson, M.D. Gilchrist, Mechanics of Composite Materials and Structures 5 (3) (1998) 291–307.
[24] N. Gupta, Materials Letters 61 (2007) 979–982.
[25] N. Gupta, W. Ricci, Materials Science and Engineering A 427 (2006) 331–342.
[26] S. Kiernan, L. Cui, M.D. Gilchrist, International Journal of Non-Linear Mechanics 44 (5) (2009) 456–468.
[27] A.H. Brothers, D.C. Dunand, Materials Science and Engineering A-Structural Materials Properties Microstructure and Processing 489 (1–2) (2008) 439–443.
[28] Y. Matsumoto, A.H. Brothers, S.R. Stock, D.C. Dunand, Materials Science and Engineering A-Structural Materials Properties Microstructure and Processing 447 (1–2) (2007) 150–157.
[29] B. Kieback, A. Neubrand, H. Riedel, Materials Science and Engineering A-Structural Materials Properties Microstructure and Processing 362 (1–2) (2003) 81–105.
[30] V.S. Deshpande, N.A. Fleck, Journal of the Mechanics and Physics of Solids 48 (6–7) (2000) 1253–1283.
[31] A.G. Hanssen, O.S. Hopperstad, M. Langseth, International Journal of Mechanical Sciences 44 (2002) 359–406.
[32] A. Reyes, O.S. Hopperstad, T. Berstad, A.G. Hanssen, M. Langseth, European Journal of Mechanics A-Solids 22 (6) (2003) 815–835.
[33] H.S. Kim, Thin-Walled Structures 40 (4) (2002) 311–327.
[34] X. Zhang, G.D. Cheng, International Journal of Impact Engineering 34 (11) (2007) 1739–1752.
[35] L. Aktay, B.H. Kroplin, A.K. Toksoy, M. Guden, Materials & Design 29 (5) (2008) 952–962.
[36] S.A. Meguid, J.C. Stranart, J. Heyerman, Finite Elements in Analysis and Design 40 (9–10) (2004) 1035–1057.
[37] S.J. Hou, Q. Li, S.Y. Long, X.J. Yang, W. Li, Finite Elements in Analysis and Design 43 (6–7) (2007) 555–565.
[38] H. Kurtaran, A. Eskandarian, D. Marzougui, N.E. Bedewi, Computational Mechanics 29 (4–5) (2002) 409–421.
[39] R. Eberhart, J. Kennedy, Proceedings of the sixth International Symposium on Micro Machine and Human Science, Nagoya, Japan, 1995, pp. 39–43.
[40] P.C. Fourie, A.A. Groenwold, Structural and Multidisciplinary Optimization 23 (4) (2002) 259–267.
[41] G.Y. Sun, G.Y. Li, Z.H. Gong, X.Y. Cui, Q. Li, Multiobjective robust optimization method for drawbead design in sheet metal forming. Materials & Design, 2009. doi:10.1016/j.matdes.2009.10.050.
[42] K.E. Parsopoulos, M.N. Vrahatis, IEEE Transactions on Evolutionary Computation 8 (3) (2004) 211–224.
[43] J. Robinson, Y. Rahmat-Samii, IEEE Transactions on Antennas and Propagation 52 (2) (2004) 397–407.
[44] A. Salman, I. Ahmad, S. Al-Madani, Microprocessors and Microsystems 26 (8) (2002) 363–371.
[45] H. Yoshida, K. Kawata, Y. Fukuyama, S. Takayama, Y. Nakanishi, IEEE Transactions on Power Systems 15 (4) (2000) 1232–1239.
[46] K.C. Lee, J.Y. Jhang, Journal of Electromagnetic Waves and Applications 20 (14) (2006) 2001–2012.
[47] D.S. Liu, K.C. Tan, C.K. Goh, W.K. Ho, Ieee Transactions on Systems Man and Cybernetics Part B-Cybernetics 37 (1) (2007) 42–50.
[48] C. Raquel, P. Naval, Proceedings of the 2005 conference on Genetic and evolutionary computation, New York, NY, USA/Washington DC, USA, 2005, pp. 257–264.
[49] A.C. Hanssen, M. Langseth, O.S. Hopperstad, International Journal of Impact Engineering 24 (5) (2000) 475–507.
[50] E.C.N. Silva, M.C. Walters, G.H. Paulino, Journal of Materials Science 41 (21) (2006) 6991–7004.